

## Article

# Assessment of Daytime HONO Emission Source from Asphalt Surface to Urban Air

Deokyoon Kim <sup>1</sup>, Jeonghwan Kim <sup>1</sup>, Meehye Lee <sup>2</sup>, Joon Young Ahn <sup>3</sup> and Gangwoong Lee <sup>1,\*</sup>

<sup>1</sup> Department of Environmental Science, Hankuk University of Foreign Studies, Yongin 17035, Korea; kdy9764@hufs.ac.kr (D.K.); kimcwjh@hufs.ac.kr (J.K.)

<sup>2</sup> Department of Earth and Environmental Sciences, Korea University, Seoul 02841, Korea; meehye@korea.ac.kr

<sup>3</sup> Division of Air Quality and Climate, National Institute of Environmental Research, Incheon 22689, Korea; nierair@korea.kr

\* Correspondence: gwlee@hufs.ac.kr

**Abstract:** Existing studies suggest various potential daytime sources of atmospheric nitrous acid (HONO), including photolysis surface reactions and photo-enhanced NO<sub>2</sub> conversion on organic surfaces. However, the understanding of daytime HONO sources is still inadequate. In this study, we report the HONO formation on asphalt surfaces under various NO<sub>2</sub>, VOCs (toluene and hexane), and UV irradiance conditions using a continuous flow chamber. Although no HONO formation was found without light exposure, the light threshold for HONO formation on the asphalt surface was very low, with a total UV (TUV) of 0.7 W m<sup>-2</sup>. HONO formation on the asphalt surface was linearly dependent on NO<sub>2</sub> up to 300 ppb in the presence of VOCs, but no HONO formation was observed with humidified air and NO<sub>2</sub>. HONO production was saturated at high hydrocarbon concentrations and light intensities. The calculated first-order NO<sub>2</sub> conversion rate to HONO on the asphalt surface was 1.2 × 10<sup>-4</sup> s<sup>-1</sup>. The observed mean HONO emission flux was 1.3 × 10<sup>9</sup> molecules cm<sup>-2</sup> s<sup>-1</sup> with a similar range of those on other urban covered surfaces. The calculated vertical HONO profile using the measured HONO emission flux and 1-D steady state model revealed that the asphalt surface may account for 13% of daytime HONO in the elevated on-road pollutant concentrations in Seoul. However, we show that its HONO contribution could be much higher on real-life road surfaces directly exposed to much higher NO<sub>2</sub> emissions from vehicle exhaust.

**Keywords:** HONO; asphalt surface; UV; VOCs; NO<sub>2</sub>



**Citation:** Kim, D.; Kim, J.; Lee, M.; Ahn, J.Y.; Lee, G. Assessment of Daytime HONO Emission Source from Asphalt Surface to Urban Air. *Appl. Sci.* **2021**, *11*, 1930. <https://doi.org/10.3390/app11041930>

Academic Editors: Elza Bontempi and Min-Suk Bae

Received: 5 January 2021

Accepted: 19 February 2021

Published: 22 February 2021

**Publisher's Note:** MDPI stays neutral with regard to jurisdictional claims in published maps and institutional affiliations.



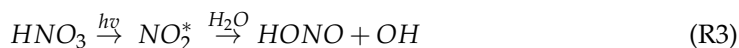
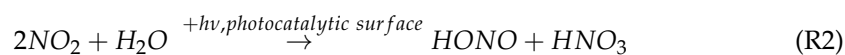
**Copyright:** © 2021 by the authors. Licensee MDPI, Basel, Switzerland. This article is an open access article distributed under the terms and conditions of the Creative Commons Attribution (CC BY) license (<https://creativecommons.org/licenses/by/4.0/>).

## 1. Introduction

Photolysis of nitrous acid (HONO) is a primary daytime source of hydroxyl radicals (OH), which are dominant atmospheric oxidants and play a significant role in the formation of ozone and secondary organic aerosol (SOA) [1,2]. The investigation of OH radical sources is crucial for understanding the tropospheric oxidation chemistry process. Therefore, many studies have investigated daytime HONO sources.

Numerous recent studies measured daytime HONO concentrations in various urban sites around the world. The observed daytime levels were unusually high, from a few hundred ppt to a few ppb, especially in China [3–6]. These results indicate that unknown dominant daytime sources of HONO, which quantitatively correspond to or exceed the photolysis rate of HONO and other loss mechanisms, are yet to be defined. The NO<sub>2</sub> dependence of heterogeneous HONO production has been well studied along with various potential formation paths, such as the reaction of NO<sub>2</sub> with water (R1) or chemisorbed water via secondary heterogeneous conversion (R2), as well as excited NO<sub>2</sub>\* from adsorbed HNO<sub>3</sub> photolysis (R3) [7].





In addition, several studies proposed HONO formation based on daytime HONO sources with large uncertainties as the mechanisms and parameters were not fully understood [2,8–11].

Recent studies suggested that the additional potential sources for daytime HONO production in urban areas are ground-level heterogeneous hydrolysis reaction with nitrate ( $\text{NO}_3^-$ ) on aerosols and building material surfaces, such as paint or glass with a thin layer of coated titanium dioxide ( $\text{TiO}_2$ ) [12,13], in the presence of humidity and UV radiation [14]. The emission rate of HONO is relatively high, especially on the surfaces of materials used in building construction that contain  $\text{TiO}_2$  particles. Other major ground-level sources reported in recent studies are HONO and NO emitted from natural soil or biological soil crusts, which are produced during nitrification and denitrification and vary with the soil pH, content of organic matter, and nutrients in the soil [15,16]. Vertical gradient studies also suggested higher HONO concentrations at ground level than at higher altitudes [17–21].

Forest canopy studies conducted in rural regions suggested a HONO production source at a higher altitude than soil emission. This source is namely the photochemical process that converts deposited  $\text{HNO}_3$  into HONO and  $\text{NO}_x$  through photolysis on the surface of tree leaves and depends considerably on the difference in acidity/pH of canopy surfaces [22]. Other daytime sources that have been reported are vehicular emissions [23], photosensitized reduction of  $\text{NO}_2$  on humic acid surfaces [24], soot [25], and photolysis of nitrate and nitric acid ( $\text{HNO}_3$ ) [26,27]. Previous studies reported that  $\text{NO}_2$  uptake coefficients and the ambient aerosol surface areas for heterogeneous conversion of  $\text{NO}_2$  were low enough to be excluded [28–30]. However, in one study conducted in Beijing [27], the average HONO production rate on aerosol was comparable to that of other sources, suggesting that aerosol significantly contributed to HONO production. Thus, HONO formation is still not fully understood.

In this study, a continuous flow chamber system was constructed to quantify HONO production on an asphalt surface based on various concentrations of  $\text{NO}_2$  and VOCs (toluene and hexane) in the presence of humidity and UV light. With the observed emission rates, the first-order conversion rate of  $\text{NO}_2$  to HONO was estimated and compared with those of other studies. In addition, HONO contributions from the asphalt surface to the daytime summer concentrations in Seoul were determined.

## 2. Experimental

### 2.1. Experimental Setup

A dynamic flow-through acrylic chamber system (45 cm × 45 cm × 20 cm) was implemented to measure HONO production on asphalt shingles (CLASSIC<sup>®</sup> SUPER, Owens Corning, Toledo, OH, USA) with  $\text{NO}_2$ , toluene, hexane, and UV light sources. Teflon (Polytetrafluoroethylene, PTFE) sheets were attached to each surface of the chamber to prevent unnecessary chemical reactions, and the chamber had a quartz window on top to allow UV-A (315–400 nm) and UV-B (280–315 nm) to enter the system. Compressed zero gas was used as the carrier gas to deliver the reactant gases through the chamber into the HONO measurement instrument described below. A dynamic dilutor connected to a standard  $\text{NO}_2$  gas cylinder (11.3 ppm) and a VOCs permeation tube was used to prepare the precursor gas mixtures. Humidity inside the chamber (50% RH) was controlled by injecting the main flow of zero gas through an impinger filled with distilled water. The total air flow rate and residence time to the chamber was approximately 15.5 LPM and 2.6 min, respectively. Light intensities were controlled by changing the distance of the xenon lamp (XG-100B, Seric., Ltd, Tokyo, Japan) from the chamber. The spectral irradiance emitted by the xenon lamp was measured with an Eppley Lab model TUVB (295–385 nm) and an Ocean Optics USB4000 spectrometer (280–950 nm). The experimental setup is presented in Figure 1.

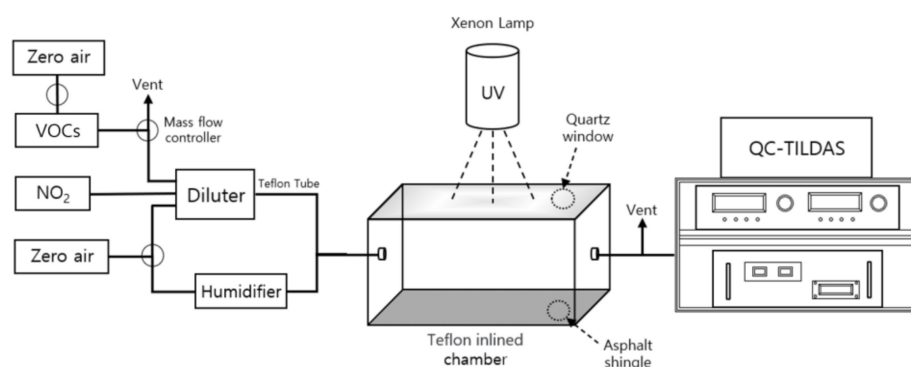


**Figure 1.** Schematic diagram of continuous flow reaction chamber setup.

## 2.2. Measurements

Highly reactive HONO was measured with a tunable infrared-laser differential absorption spectrometer (TILDAS) with applied quantum cascade (QC) lasers. QC-TILDAS, developed by the Aerodyne Research Incorporation, is designed for measuring real-time HONO with a high sensitivity ( $\sim 0.1$  ppbv) and short response time (1–10 Hz). It determines the mixing ratio of the measured trace gases by monitoring the absorption of the molecule's radiation at  $1273\text{ cm}^{-1}$  for measuring HONO. The absorption amount was then compared with the theoretical spectrum of the High-resolution TRANsmision (HITRAN) database to calculate the mixing ratio of HONO. The TDL Wintel data acquisition program installed in the instrument is designed to perform a frequency scan and acquire the resulting absorption spectrum for analysis of the spectra obtained by QC-TILDAS [31]. Dry  $\text{N}_2$  (99.999%) background gas was injected at 5-min intervals to clean out the multipass cell (MPC) while stabilizing the baseline for measurement.

The productions of HONO from the surfaces inside of the chamber were tested along with varying  $\text{NO}_2$  concentrations (up to 300 ppbv) under  $11.3\text{ W m}^{-2}$  of TUV and 500 ppbv of toluene. The highest measured HONO concentration in the blank tests was 0.01 ppbv, which is below the detection limit ( $\sim 0.1$  ppbv) of QC-TILDAS. Although we couldn't quantify the exact HONO productions in our chamber surfaces due to analytical limitation, it was possible to assume that they were zero, or at most, they statistically insignificant.

Field observations were performed with QC-TILDAS at two different locations in Seoul, Korea. The first field study was conducted during the KORea USa–Air Quality (KORUS-AQ) campaign from May 19 to June 12, 2016; a container top at the Olympic Park site ( $37.52^\circ\text{ N}$ ,  $127.12^\circ\text{ E}$ ), which has dense vegetation and is located in a highly populated area with heavy traffic surrounding the park, was studied. Another study was conducted on the fourth floor of a building ( $37.59^\circ\text{ N}$ ,  $127.08^\circ\text{ E}$ ), located in a commercial area of Jungnang district with high levels of traffic and large buildings surrounding the measurement site, from May 1 to June 9, 2019.

## 2.3. Conversion Rate of $\text{NO}_2$ to HONO

In our chamber reaction setup with a continuous flow rate ( $f$ ), the conversion rate of  $\text{NO}_2$  to HONO,  $R_{\text{HONO}}$ , on the asphalt surface can be expressed by a first-order reaction rate constant ( $k_{\text{HONO}}$ ) and input  $\text{NO}_2$  concentration. This rate can be estimated with a simple molar balance of the entering ( $C_i$ ) and exiting HONO concentrations ( $C_o$ ) within the chamber volume ( $V$ ) as in (1).

$$R_{\text{HONO}} = k_{\text{hono}} \bullet \text{NO}_2 = \frac{(C_o - C_i) \bullet f}{V} \quad (1)$$

As the initial HONO concentration ( $C_i$ ) is zero,  $k_{HONO}$  can be calculated using Equation (2) from the ratio between produced HONO and initial  $NO_2$ , flow rate, and chamber volume.

$$k_{hono} = \frac{(C_o - C_i) \bullet f}{NO_2 \bullet V} = \frac{C_o \bullet f}{NO_2 \bullet V} = \alpha \frac{f}{V} \quad (2)$$

### 3. Results

#### 3.1. UV Irradiance Dependency

HONO production on asphalt shingle surfaces was evaluated along with changes in UV intensity,  $NO_2$ , and VOC concentrations. As three factors were taken into account, we evaluated one factor at a time while keeping all other factors fixed to typical values. Figure 2 shows the observed HONO production on the asphalt surface with varying UV intensities in the constant flow chamber reactor with humidified air, with 100 ppbv of  $NO_2$  and 500 ppbv of toluene. The observed HONO production ranged from zero to a maximum of  $1.4 \times 10^9$  molecules  $cm^{-2} s^{-1}$  at UV (295–385 nm) irradiance of  $11.3 W/m^2$ , which is typical daytime UV irradiance during the summer in Korea. The error bars indicate standard deviations of triplicate readings. Interestingly, HONO production increased sharply within a very narrow range under very low light conditions.

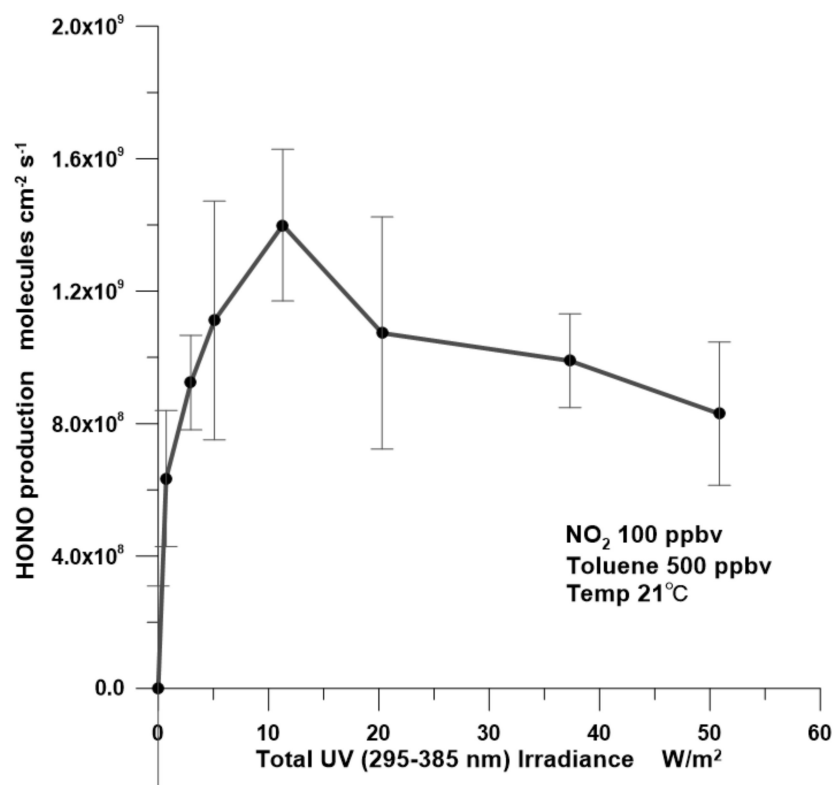


**Figure 2.** HONO production rate as a function of total UV irradiance. Input concentrations of  $NO_2$  and toluene were fixed as 100 ppbv and 500 ppbv, respectively.

In this experiment, no emission of HONO was observed in the dark, confirming that the proposed reaction is activated with photon fluxes. However, the UV light threshold to initiate photolytic HONO production on the asphalt surface was very low. Even at the lowest UV irradiance at  $0.7 W/m^2$ , substantial formation of HONO over  $6 \times 10^8$  molecules  $cm^{-2} s^{-1}$  was observed. This UV intensity was close to that observed in the early morning or late afternoon. Observed efficient HONO production under this low-light condition implies that HONO emission from the asphalt surface is an important additional OH source near the ground, especially in the early morning and late afternoon when other OH sources are limited.

HONO production peaked at  $11.3 \text{ Wm}^{-2}$  and then decreased slowly with UV intensity. The decrease in HONO production rate at higher UV intensities is likely due to two reasons. One is increasing HONO decomposition, which is proportional to the actinic flux [32]. Another is the deactivation of photo-produced reduced species on the asphalt surface by photo-oxidant species, which are formed simultaneously during high light intensity [24]. Hereafter, we fixed the integrated UV (295–385 nm) intensity at  $11.3 \text{ Wm}^{-2}$  to test the effects of  $\text{NO}_2$  and VOCs on HONO production.

### 3.2. $\text{NO}_2$ Dependency

Figure 3 shows the results of the experiment conducted to elucidate the  $\text{NO}_2$  contribution to HONO production over the asphalt surface. HONO formation on the asphalt surface was linearly dependent on  $\text{NO}_2$  up to 300 ppbv. As shown in Figure 2, HONO formation was not observed in dark conditions even with relatively high  $\text{NO}_2$  concentrations, which indicates that heterogeneous  $\text{NO}_2$  conversion with  $\text{H}_2\text{O}$  is not a source of HONO over the asphalt surface. This result is not similar or analogous with glass surface studies, in which photo-enhancement of the reaction was not observed [7,19,33]. However, it is in good agreement with the results of a light-induced HONO formation study on aerosol surfaces [28,34,35].

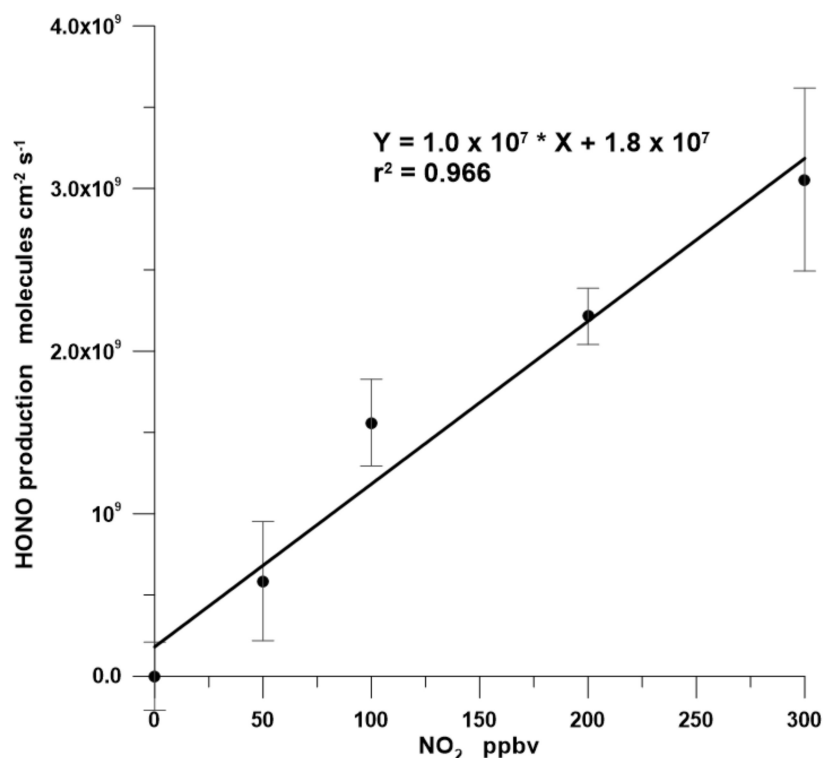


**Figure 3.** HONO production rates as functions of  $\text{NO}_2$  concentrations. Mixing ratios of toluene and total ultraviolet (TUV) were fixed as 500 ppbv and  $11.3 \text{ Wm}^{-2}$ , respectively.

Photochemical HONO formation has been mainly suggested as a reaction of adsorbed  $\text{NO}_2$  on the photocatalytic surface, such as  $\text{TiO}_2$  and humic acid [28,33]. Another potential HONO formation reaction is the photolysis of excited  $\text{NO}_2^*$  originating from the  $\text{HNO}_3$  complex with water. Using our experimental setup without  $\text{NO}_2$ , no HONO production was observed, indicating that  $\text{HNO}_3$  photolysis does not play a significant role in HONO formation with an asphalt surface. This implies that the observed HONO production on the asphalt surface is mainly caused by the heterogeneous photoactivated ions of  $\text{NO}_2$  by a similar reaction on the humic acid as proposed by Stemmler et al. [28] (R4).



### 3.3. Conversion Rate of NO<sub>2</sub> to HONO

According to Equations (1) and (2) under the conditions of 11.3 W m<sup>-2</sup> of UV intensity and 500 ppbv of toluene, we calculated  $k_{HONO}$  (the first-order NO<sub>2</sub> conversion rate to HONO) of  $1.23 \times 10^{-4} \text{ s}^{-1}$  for the asphalt surface, which is much smaller than a commercial TiO<sub>2</sub>-doped paint surface [34]. The HONO emission fluxes in our experiment range between zero and  $3.1 \times 10^9 \text{ molecules cm}^{-2} \text{ s}^{-1}$  along with NO<sub>2</sub> concentrations (Figure 3). In Table 1, the observed HONO fluxes with the asphalt surface are compared with other common surfaces found in urban conditions. The HONO emission fluxes on TiO<sub>2</sub> photocatalytic paint surface studies are 10 times higher than that of the asphalt surface.

**Table 1.** Comparison of HONO emission rate on surfaces of various materials.

Material	Emission Rate (Molecules cm <sup>-2</sup> s <sup>-1</sup> )	NO <sub>2</sub> (ppb)	RH (%)	Irradiance (W m <sup>-2</sup> )	Wavelength (nm)	RF	
Paint	White wall paint	$1.3 \times 10^{10}$	50	50	10.6	300–400	[35]
	Photocatalytic paint (3.5% TiO <sub>2</sub> nanoparticles)	$2.1 \times 10^{10}$	40	40	8.5	340–400	[36]
Glass	Clean	$1.3 \times 10^9$	50	50	10.6	300–400	[35]
	Urban grime	$1.5 \times 10^{10}$	46	90	8.0	300–400	[37]
Aerosol		$2.5 \times 10^9$		60		400 < λ	[27]
Soil		$2.2 \times 10^{11}$					[37]
		$1.3 \times 10^8$					[38]
		$1.5 \times 10^9$					[39]
		$2.4 \times 10^9$					[39]
		$6.2 \times 10^9$					[40]
Forest canopy		$6.0 \times 10^8$					[18]
		$6.7 \times 10^9$					[26]
		$3.3 \times 10^9$					[20]
							This study
Asphalt		$0.5\text{--}3.1 \times 10^9$	50–300	50	11.3	295–385	This study

Several studies reported high HONO production on aerosol surfaces with large components of photoreactive humic acids and soots [41]. Although a few high fluxes of HONO on soil, forest canopy, and TiO<sub>2</sub> paint studies were reported, HONO emission flux from asphalt surfaces in this study is generally in a similar range as those on other common urban surfaces such as glass, aerosol, soil, and forest canopies. This implies that HONO production with heterogeneous photolytic NO<sub>2</sub> conversion from asphalt surfaces is likely an important source of daytime HONO, especially in urban areas.

### 3.4. VOCs Dependency

We measured the HONO production rate changes with varying toluene and hexane concentrations to test VOCs' role in the HONO production (Figure 4). Without toluene and hexane addition, no detectable amount of HONO production on the asphalt surface was observed in the chamber reaction with humidified air of 100 ppbv NO<sub>2</sub> under typical daylight conditions.

If the HONO production mechanism on the asphalt surface is same as that on humic acid as reaction (R4), HONO can be produced only by NO<sub>2</sub> with light. Adding 100 ppbv of VOCs under the same NO<sub>2</sub> and light conditions, HONO production became clearly efficient at a rate of  $5.2 \times 10^8 \text{ molecules cm}^{-2} \text{ s}^{-1}$ . HONO production rapidly increased with toluene and hexane concentrations up to 500 ppbv and then became saturated at higher concentrations. Heterogeneous HONO production on photocatalytic mineral surfaces such as TiO<sub>2</sub> and humic acid is driven by a hydrogen source from water or humic acid itself. Thus, the observed toluene and hexane dependence of the HONO production rate in this study requires a different reaction path than reaction (R4) alone.

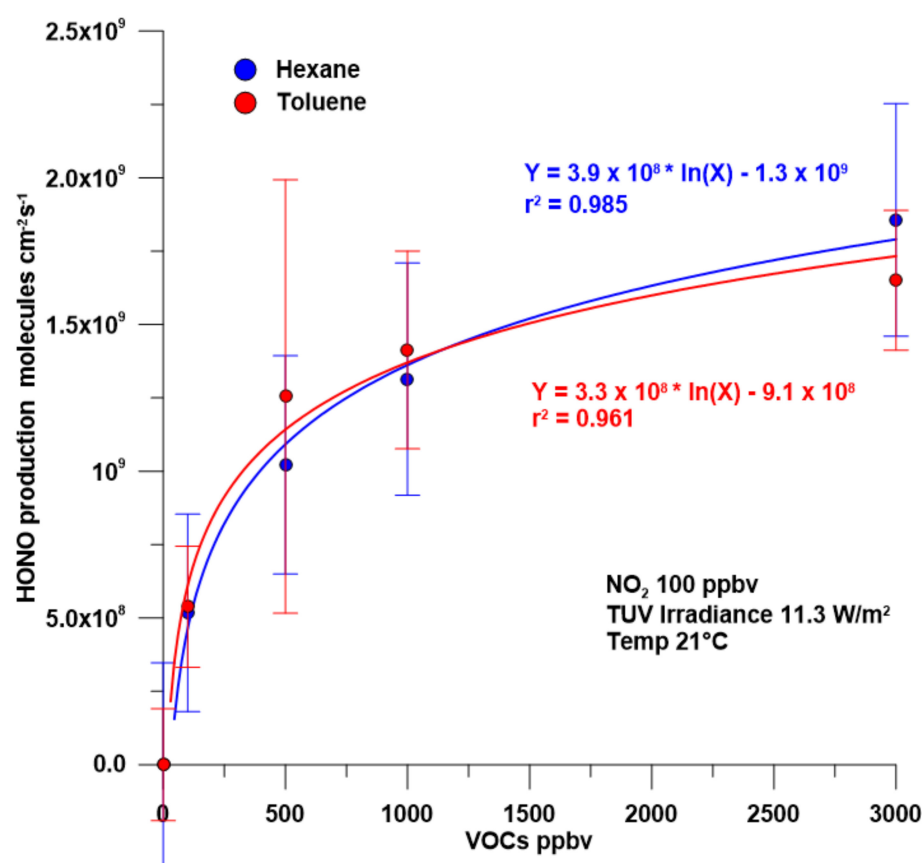


**Figure 4.** HONO production rates as a function of toluene and hexane mixing ratios.  $\text{NO}_2$  and TUV were fixed as 100 ppbv and  $11.3 \text{ W m}^{-2}$ , respectively.

The asphalt surfaces used in this experiment are highly complex mixtures of organics and inorganics. In particular, the organic composition, mainly from petroleum in the sedimentary source, is not well characterized owing to many different geographical origins and refining processes. As asphalt from crude oil is a derivative of humic acids, asphalt has structural similarities with humic acids having numerous aromatic rings. In contrast to universal polycyclic structures, humic acids contain higher contents of oxidized and polar branches, such as alcohols and carbonates compared to asphalt. For this reason, humic acids are extremely hydrophilic, but the asphalt surface is very hydrophobic. The hydrophobic nature of the asphalt surface is likely to abate the water uptake to its surface, which may cause a much lower rate of HONO formation compared to the humic acid surface under humidified air conditions. However, VOCs and its oxidized derivatives can be easily absorbed to the asphalt surface and they can be an effective hydrogen source on the asphalt surface.

In addition, it was reported that  $\text{NO}_2$  conversion on humic acid surfaces was not proportional to the high light intensities [28] and even saturated in the light of early morning hours [39]. As stated earlier, substantial formation of HONO on the asphalt surface under low light conditions and then rapid saturation in typical daylight indicate that the asphalt surface has a light dependency similar to that of the humic acid surface [28], in contrast to photocatalytic mineral surfaces where HONO formation is linear for a wide range of light intensities [36].

These distinct characteristics of VOCs dependency on HONO formation observed in our experiment strongly suggest that the HONO production mechanism on hydrophobic asphalt surfaces is different with that on typical hydrophilic humic acid surfaces. In this condition, hydrocarbons and its oxidized derivatives may act as hydrogen donors on the hydrophobic asphalt surface and enhance the reduction of  $\text{NO}_2$  to HONO by a process

similar to that proposed by Han et al. [42] (R5). Consequently, the saturated HONO production on the asphalt surface at higher VOCs concentrations can be attributed to the limited oxidation of VOCs under fixed conditions of light intensity and NO<sub>2</sub> concentration.



Given that our experiments were not designed to analyze the detailed mechanism of HONO formation on the asphalt surface, our postulate cannot be fully proven at this stage and needs to be tested in further studies. The purpose of this study was to assess the contributions of HONO flux from asphalt surface to daytime HONO concentrations in typical urban conditions.

### 3.5. Vertical Profile of HONO above the Asphalt Surface

Table 2 shows observed daytime HONO concentrations in selected urban areas, including two field studies in Seoul performed in this study. It confirms again that substantial amounts of daytime HONO could not be accounted only for well-identified homogeneous HONO formation with NO and OH in urban areas.

**Table 2.** Comparison of daytime HONO concentration at various urban sites around the world (unit: ppbv).

Location	Sampling Period	Instrument	Min	Mean	Max	Reference
London, UK	July–Aug 2012	LOPAP <sup>a</sup>	0.20	0.44	0.60	[43]
New York, USA	July–Aug 2001	HPLC <sup>b</sup>	0.40	0.46	1.40	[44]
Houston, USA	Apr 21, 2009	LP-DOAS <sup>c</sup>	0.05	0.1	0.15	[21]
Bakersfield, USA	May–July, 2010	AIM <sup>d</sup>	0.03	0.08	0.13	[19]
Beijing, China	Aug 2007	UV-Vis	0.80	-	1.60	[45]
	July 2008–April 2009	MAX-DOAS <sup>e</sup>	0.1	0.36	0.8	[46]
Jinan, China	Nov 2013–Jan 2014	WRD <sup>f</sup>	0.16	-	0.58	[47]
	Sep 2015–Aug 2016	LOPAP	0.02	0.99	7.39	[4]
Seoul, Korea	May–June 2016	QC-TILDAS <sup>g</sup>	0.20	0.60	1.47	This study
	May–June 2019	QC-TILDAS	0.01	0.45	1.20	This study

<sup>a</sup> Long path absorption photometer. <sup>b</sup> High-performance liquid chromatography. <sup>c</sup> Long-path differential optical absorption spectrometer.

<sup>d</sup> Ambient ion monitoring system. <sup>e</sup> Multi-axis differential optical absorption spectrometer. <sup>f</sup> Wet rotating denuder. <sup>g</sup> Quantum cascade-tunable infrared-laser differential absorption spectrometer.

Observed HONO means in Seoul were 0.6 and 0.45 ppbv at Olympic Park site during the 2016 KORUS-AQ campaign and at an urban site of Jungrang district in 2019, respectively. These values in Seoul are in the middle range of typical urban conditions. We attempted to determine the fraction of HONO that can be explained by asphalt-surface HONO production. If we exclude other HONO sources and sinks, such as gaseous HONO formation (NO+OH) and other ground and aerosol sources and sinks, then the changing rate of daytime HONO formation can be expressed using vertical eddy transport, photolysis of HONO, and asphalt surface production, as shown in Equation (3).

$$\frac{\partial[\text{HONO}]}{\partial t} = -\frac{\partial}{\partial z} \left( K_z \frac{\partial[\text{HONO}]}{\partial z} \right) - J_{\text{hono}}[\text{HONO}] + \text{Flux}_{\text{asphalt surface}} \quad (3)$$

If we assume that the HONO concentration is in a steady state ( $\frac{\partial[\text{HONO}]}{\partial t} = 0$ ), then we can solve the 1-D differential Equation (3) with flux boundary conditions using the forward Euler method with discretizing diffusion operators for allowable time steps. Implementation of numerical computations for Equation (3) requires additional known parameters, such as eddy diffusivity ( $K_z$ ), photolysis rate of HONO ( $J_{\text{hono}}$ ), and asphalt surface flux of HONO ( $\text{Flux}_{\text{asphalt surface}}$ ). Based on typical summer meteorological conditions during the study period, the atmosphere in the boundary layer is generally considered to be moderately unstable. We estimated the vertical diffusivities ( $K_z$ ) along with heights using a simplified diffusivity profile derived from a nonhydrostatic, semi-implicit model for a mod-

erately unstable 1-km boundary layer [48–50], as shown in Figure 5. The photolysis rate of HONO ( $J_{\text{hono}}$ ) was set to a constant value of  $0.0017 \text{ s}^{-1}$  for typical daytime light conditions.

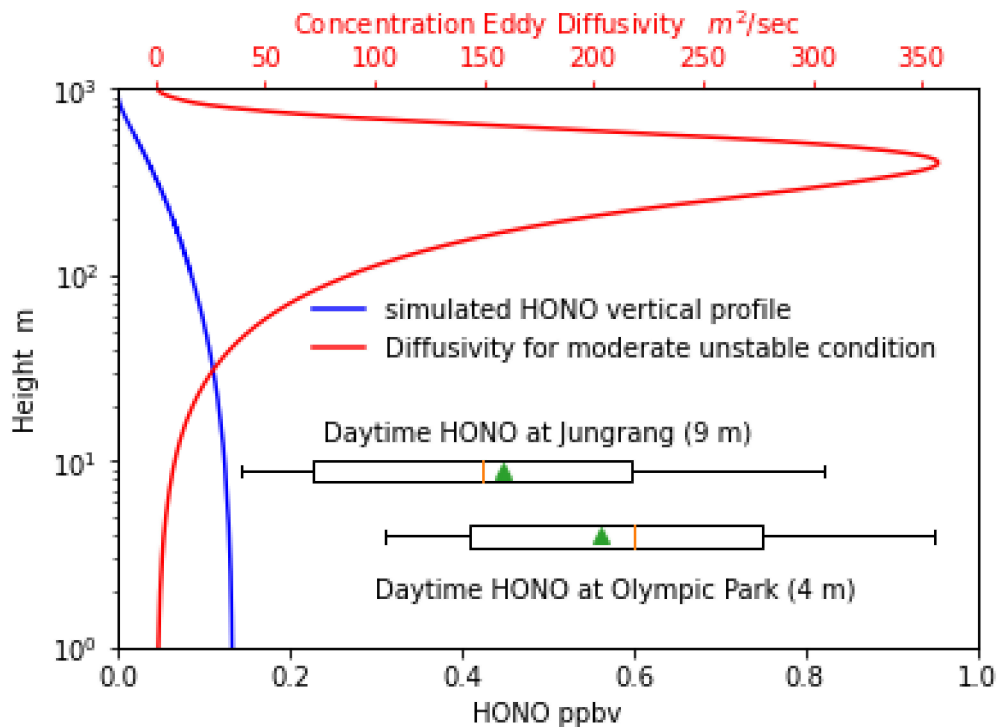


**Figure 5.** Estimated HONO concentration vertical diffusivity in red color and calculated vertical profile of daytime HONO in blue color compared with measured HONO of means (green triangle), medians and percentiles (10th, 25th, 75th, and 90th) for two field observations in Seoul, both with heights on logarithmic scale.

To estimate the average value of the asphalt-surface HONO flux in Seoul, we built a random forest regression model and a least square regression model with dependent variables (HONO asphalt surface flux) and controlled features ( $\text{NO}_2$ , VOCs, and UV intensities) of the independent variables. The model-calculated HONO flux values were well matched with experimental data with r-square of 0.932 and 0.931 for random forest regression and a least square model, respectively. Using these models, we estimated an asphalt surface HONO flux of  $1.3 \times 10^9 \text{ molecules cm}^{-2} \text{ s}^{-1}$  for on-road pollutant conditions with 160 ppbv for  $\text{NO}_2$  and 100 ppbv for total hydrocarbons (TVOCs) observed in tunnel studies in Seoul, which are three to five times higher than those found in the roadside [51,52].

Figure 5 also depicts the simulated vertical profile of daytime HONO and the observed HONO of medians and percentiles (10th, 25th, 75th, and 90th) for the two field measurements in Seoul. While the simulated HONO shows a maximum of 0.13 ppbv at the ground level, it decreases slowly within the surface layer of a few tens of meters, which is obviously affected by well-mixed air characteristics under unstable weather conditions in the summer.

This profile was computed with the assumption of steady-state HONO equilibrated only on the asphalt surface production. The fraction of asphalt paved roads is 13.7% of the total surface area in Seoul. The percentage is much higher, up to 50%, in the downtown area, and the unknown but significant amount of urban roof surface is also covered with asphalt shingles. For these reasons, the calculated vertical HONO profile cannot be overestimated by more than a factor of two. If we consider all of these uncertainty factors together, then we can conclude that asphalt-surface HONO formation may attribute up to 0.07 ppbv of HONO near the ground level, which is about 13% of daytime HONO in Seoul. The

results suggest that the majority of daytime HONO is formed by unknown sources such as aerosols, photoreactive minerals, ground sources with soils, or vegetated surfaces.

It should be noted that HONO formation on the asphalt surface in this study was tested with precursor concentrations observed in the tunnel. In a real scenario, we can expect a much higher HONO formation rate on the asphalt road surface as it is directly exposed to vehicle exhaust containing ppm levels of NO<sub>2</sub> and hydrocarbons. Fixing all other factors, our data show that the HONO formation rate on the asphalt surface increases proportionally to the NO<sub>2</sub> concentration. This implies that HONO production on the asphalt surface may play a significant role in daytime HONO production in urban areas, especially where the real road surface is exposed to the immediate emission of NO<sub>2</sub> and hydrocarbons from vehicle exhaust. It is necessary to note that HONO formation on asphalt surfaces was not tested under real traffic conditions; thus, further detailed analysis must be performed considering traffic conditions. Additional efforts are needed to assess comprehensive mechanisms of surface HONO production on asphalt and its contributions to daytime HONO in urban areas in the future.

#### 4. Conclusions

Photolytic HONO formations on an asphalt surface were tested along with the factors influencing the formation by using a continuous flow chamber system. The contributions of these factors to ambient daytime HONO concentrations observed during the summers of 2016 and 2019 in Seoul were assessed. The daytime means of observed HONO were 0.60 and 0.45 ppbv at two different locations in Seoul. These values are comparable to other urban conditions and strongly suggest that some common daytime HONO sources exceed the rapid daytime HONO sinks.

HONO production was evaluated using three factors on the asphalt surface within an experiment chamber: UV intensity, NO<sub>2</sub> concentration, and VOCs (toluene and hexane) concentration. HONO was not generated on the asphalt surface if any of these parameters were low, which confirms that these are all critical parameters in asphalt surface reactions. Although no HONO surface formation was found in the no-light condition, significant HONO formation of  $6 \times 10^8$  molecules cm<sup>-2</sup> s<sup>-1</sup> was observed even under very low radiation of UV (0.7 W m<sup>-2</sup>). This shows that the asphalt surface may be an important source of HONO in the early morning and late afternoon when other photoreactive sources are not readily available.

We found that HONO formation on the asphalt surface was linearly dependent on NO<sub>2</sub>. Moreover, we calculated the first-order conversion rate of NO<sub>2</sub> to HONO for  $1.2 \times 10^{-4}$  s<sup>-1</sup>, which is two orders smaller than those of a TiO<sub>2</sub>-doped surface. No HONO formation on the asphalt surface was observed with humidified air and high-NO<sub>2</sub> conditions, unlike for other photoreactive minerals such as TiO<sub>2</sub>.

Saturated HONO production at high hydrocarbon concentrations and high light intensities was another distinct characteristic of the asphalt surface reaction. These results suggested that the HONO production mechanism on the asphalt surface was similar with that on the humic acid surface. However, the low oxygen content and hydrophobic nature of the asphalt surface were less efficient than humic acid surfaces in producing HONO, and substantial addition of hydrocarbons was needed to produce HONO, unlike in the case of humic acid.

The observed HONO emission flux of  $1.3 \times 10^9$  molecules cm<sup>-2</sup> s<sup>-1</sup> under typical on-road conditions was much smaller than that of highly photoreactive mineral and organic surfaces, but it was in a similar range to that of other urban covered surfaces such as glass and soils. This implies that HONO production with heterogeneous photolytic NO<sub>2</sub> conversion from asphalt surfaces is a likely important source of daytime HONO in most urban areas.

Numerically simulated vertical HONO profiles with obtained asphalt emission sources revealed that the asphalt surface may account for 13% of daytime HONO in the typical roadside precursor concentrations in Seoul. However, this number could be higher, given

that NO<sub>2</sub> and hydrocarbon concentrations on the road asphalt surface are larger as they are directly exposed to emissions from vehicle exhaust and tailpipes. Overall, these results indicate a potentially significant daytime source of HONO in urban areas and propose a need for further analysis of the formation mechanism and its contributions to daytime HONO in real traffic conditions.

**Author Contributions:** Conceptualization and methodology, G.L., M.L. and J.Y.A.; formal analysis, D.K. and J.K.; investigation, D.K., J.K., G.L.; resources, G.L. and J.Y.A.; data curation, D.K., J.K.; writing—original draft preparation, D.K., J.K. and G.L.; writing—review and editing, M.L.; visualization, D.K., J.K., G.L. All authors have read and agreed to the published version of the manuscript.

**Funding:** This research was funded by National Research Foundation of Korea (NRF), grant number 2018R1A2B6005090.

**Institutional Review Board Statement:** Not applicable.

**Informed Consent Statement:** Not applicable.

**Data Availability Statement:** The data presented in this study are available on request from the corresponding author.

**Conflicts of Interest:** The authors declare no conflict of interest.

## References

1. Hofzumahaus, A.; Rohrer, F.; Lu, K.; Bohn, B.; Brauers, T.; Chang, C.C.; Fuchs, H.; Holland, F.; Kita, K.; Kondo, Y.; et al. Amplified trace gas removal in the troposphere. *Science* **2009**, *324*, 1702–1704. [[CrossRef](#)]
2. Li, G.; Lei, W.; Zavala, M.; Volkamer, R.; Dusanter, S.; Stevens, P.; Molina, L.T. Impacts of HONO sources on the photochemistry in Mexico City during the MCMA-2006/MILAGO Campaign. *Atmos. Chem. Phys.* **2010**, *10*, 6551–6567. [[CrossRef](#)]
3. Wang, S.; Zhou, R.; Zhao, H.; Wang, Z.; Chen, L.; Zhou, B. Long-term observation of atmospheric nitrous acid (HONO) and its implication to local NO<sub>2</sub> levels in Shanghai, China. *Atmos. Environ.* **2013**, *77*, 718–724. [[CrossRef](#)]
4. Li, D.; Xue, L.; Wen, L.; Wang, X.; Chen, T.; Mellouki, A.; Chen, J.; Wang, W. Characteristics and sources of nitrous acid in an urban atmosphere of northern China: Results from 1-yr continuous observations. *Atmos. Environ.* **2018**, *182*, 296–306. [[CrossRef](#)]
5. Hao, Q.; Jiang, N.; Zhang, R.; Yang, L.; Li, S. Characteristics, sources, and reactions of nitrous acid during winter at an urban site in the Central Plains Economic Region in China. *Atmos. Chem. Phys.* **2020**, *20*, 7087–7102. [[CrossRef](#)]
6. Liu, Y.; Zhang, Y.; Lian, C.; Yan, C.; Feng, Z.; Zheng, F.; Fan, X.; Chen, Y.; Wang, W.; Chu, B.; et al. The promotion effect of nitrous acid on aerosol formation in wintertime Beijing: Possible contribution of traffic-related emission. *Atmos. Chem. Phys.* **2020**, 1–43. [[CrossRef](#)]
7. Laufs, S.; Kleffmann, J. Investigations on HONO formation from photolysis of adsorbed HNO<sub>3</sub> on quartz glass surfaces. *Phys. Chem. Chem. Phys.* **2016**, *18*, 9616–9625. [[CrossRef](#)]
8. Czader, B.H.; Rappengü Uck, B.; Percell, P.; Byun, D.W.; Ngan, F.; Kim, S. Modeling nitrous acid and its impact Atmospheric Chemistry and Physics Discussions Modeling nitrous acid and its impact on ozone and hydroxyl radical during the Texas Air Quality Study 2006 Modeling nitrous acid and its impact Modeling nitrous acid and its impact. *Atmos. Chem. Phys. Discuss* **2012**, *12*, 5851–5880. [[CrossRef](#)]
9. Gonçalves, M.; Dabdub, D.; Chang, W.L.; Jorba, O.; Baldasano, J.M. Impact of HONO sources on the performance of mesoscale air quality models. *Atmos. Environ.* **2012**, *54*, 168–176. [[CrossRef](#)]
10. Kleffmann, J. Daytime sources of nitrous acid (HONO) in the atmospheric boundary layer. *ChemPhysChem.* **2007**, *8*, 1137–1144. [[CrossRef](#)]
11. Spataro, F.; Ianniello, A. Sources of atmospheric nitrous acid: State of the science, current research needs, and future prospects. *J. Air Waste Manag. Assoc.* **2014**, *64*, 1232–1250. [[CrossRef](#)] [[PubMed](#)]
12. Bartolomei, V.; Sörgel, M.; Gligorovski, S.; Alvarez, E.G.; Gandolfo, A.; Strekowski, R.; Quivet, E.; Held, A.; Zetzsch, C.; Wortham, H. Formation of indoor nitrous acid (HONO) by light-induced NO<sub>2</sub> heterogeneous reactions with white wall paint. *Environ. Sci. Pollut. Res.* **2014**, *21*, 9259–9269. [[CrossRef](#)] [[PubMed](#)]
13. Langridge, J.M.; Gustafsson, R.J.; Griffiths, P.T.; Cox, R.A.; Lambert, R.M.; Jones, R.L. Solar driven nitrous acid formation on building material surfaces containing titanium dioxide: A concern for air quality in urban areas? *Atmos. Environ.* **2009**, *43*, 5128–5131. [[CrossRef](#)]
14. Li, S.; Matthews, J.; Sinha, A. Atmospheric hydroxyl radical production from electronically excited NO<sub>2</sub> and H<sub>2</sub>O. *Science* **2008**, *319*, 1657–1660. [[CrossRef](#)] [[PubMed](#)]
15. Meusel, H.; Tamm, A.; Kuhn, U.; Wu, D.; Leifke, A.L.; Fiedler, S.; Ruckteschler, N.; Yordanova, P.; Lang-Yona, N.; Pöhlker, M.; et al. Emission of nitrous acid from soil and biological soil crusts represents an important source of HONO in the remote atmosphere in Cyprus. *Atmos. Chem. Phys.* **2018**, *18*, 799–813. [[CrossRef](#)]

16. Oswald, R.; Behrendt, T.; Ermel, M.; Wu, D.; Su, H.; Cheng, Y.; Breuninger, C.; Moravek, A.; Mougin, E.; Delon, C.; et al. HONO emissions from soil bacteria as a major source of atmospheric reactive nitrogen. *Science* **2013**, *341*, 1233–1235. [[CrossRef](#)]
17. Kleffmann, J.; Kurtenbach, R.; Lörzer, J.; Wiesen, P.; Kalthoff, N.; Vogel, B.; Vogel, H. Measured and simulated vertical profiles of nitrous acid - Part I: Field measurements. *Atmos. Environ.* **2003**, *37*, 2949–2955. [[CrossRef](#)]
18. Ren, X.; Sanders, J.E.; Rajendran, A.; Weber, R.J.; Goldstein, A.H.; Pusede, S.E.; Browne, E.C.; Min, K.-E.; Cohen, R.C. A relaxed eddy accumulation system for measuring vertical fluxes of nitrous acid. *Atmos. Meas. Tech.* **2011**, *4*, 2093–2103. [[CrossRef](#)]
19. VandenBoer, T.C.; Markovic, M.Z.; Sanders, J.E.; Ren, X.; Pusede, S.E.; Browne, E.C.; Cohen, R.C.; Zhang, L.; Thomas, J.; Brune, W.H.; et al. Evidence for a nitrous acid (HONO) reservoir at the ground surface in Bakersfield, CA, during CalNex 2010. *J. Geophys. Res. Atmos.* **2014**, *119*, 9093–9106. [[CrossRef](#)]
20. Zhou, X.; Zhang, N.; Teravest, M.; Tang, D.; Hou, J.; Bertman, S.; Alaghmand, M.; Shepson, P.B.; Carroll, M.A.; Griffith, S.; et al. Nitric acid photolysis on forest canopy surface as a source for tropospheric nitrous acid. *Nat. Geosci.* **2011**, *4*, 440–443. [[CrossRef](#)]
21. Wong, K.W.; Tsai, C.; Lefer, B.; Haman, C.; Grossberg, N.; Brune, W.H.; Ren, X.; Luke, W.; Stutz, J. Daytime HONO vertical gradients during SHARP 2009 in Houston, TX. *Atmos. Chem. Phys.* **2012**, *12*, 635–652. [[CrossRef](#)]
22. Zhang, N.; Zhou, X.; Bertman, S.; Tang, D.; Alaghmand, M.; Shepson, P.B.; Carroll, M.A. Measurements of ambient HONO concentrations Atmospheric Chemistry and Physics Discussions Measurements of ambient HONO concentrations and vertical HONO flux above a northern Michigan forest canopy Measurements of ambient HONO concentrations. *Atmos. Chem. Phys. Discuss* **2012**, *12*, 7273–7304. [[CrossRef](#)]
23. Nakashima, Y.; Sadanaga, Y.; Saito, S.; Hoshi, J.; Ueno, H. Contributions of vehicular emissions and secondary formation to nitrous acid concentrations in ambient urban air in Tokyo in the winter. *Sci. Total Environ.* **2017**, *592*, 178–186. [[CrossRef](#)]
24. Stemmler, K.; Ammann, M.; Donders, C.; Kleffmann, J.; George, C. Photosensitized reduction of nitrogen dioxide on humic acid as a source of nitrous acid. *Nature* **2006**, *440*, 195–198. [[CrossRef](#)]
25. Guan, C.; Li, X.; Zhang, W.; Huang, Z. Identification of nitration products during heterogeneous reaction of NO<sub>2</sub> on soot in the dark and under simulated sunlight. *J. Phys. Chem. A* **2017**, *121*, 482–492. [[CrossRef](#)] [[PubMed](#)]
26. Ye, C.; Gao, H.; Zhang, N.; Zhou, X. Photolysis of Nitric Acid and Nitrate on Natural and Artificial Surfaces. *Environ. Sci. Technol.* **2016**, *50*, 46. [[CrossRef](#)]
27. Bao, F.; Li, M.; Zhang, Y.; Chen, C.; Zhao, J. Photochemical Aging of Beijing Urban PM<sub>2.5</sub>: HONO Production. *Environ. Sci. Technol.* **2018**, *52*, 6309–6316. [[CrossRef](#)] [[PubMed](#)]
28. Stemmler, K.; Ndour, M.; Elshorbany, Y.; Kleffmann, J.; D’Anna, B.; George, C.; Bonn, B.; Ammann, M. Light induced conversion of nitrogen dioxide into nitrous acid on submicron humic acid aerosol. *Atmos. Chem. Phys.* **2007**, *7*, 4237–4248. [[CrossRef](#)]
29. Sarwar, G.; Roselle, S.J.; Mathur, R.; Appel, W.; Dennis, R.L.; Vogel, B. A comparison of CMAQ HONO predictions with observations from the Northeast Oxidant and Particle Study. *Atmos. Environ.* **2008**, *42*, 5760–5770. [[CrossRef](#)]
30. Zhang, L.; Wang, T.; Zhang, Q.; Zheng, J.; Xu, Z.; Lv, M. Potential sources of nitrous acid (HONO) and their impacts on ozone: A WRF-Chem study in a polluted subtropical region. *J. Geophys. Res.* **2016**, *121*, 3645–3662. [[CrossRef](#)]
31. Lee, B.H.; Wood, E.C.; Wormhoudt, J.; Shorter, J.H.; Herndon, S.C.; Zahniser, M.S.; Munger, J.W. Effective line strengths of trans-nitrous acid near 1275cm<sup>-1</sup> and cis-nitrous acid at 1660cm<sup>-1</sup>. *J. Quant. Spectrosc. Radiat. Transf.* **2012**, *113*, 1905–1912. [[CrossRef](#)]
32. Wall, K.J.; Schiller, C.L.; Harris, G.W. Measurements of the HONO photodissociation constant. *J. Atmos. Chem.* **2006**, *55*, 31–54. [[CrossRef](#)]
33. Chen, H.; Nanayakkara, C.E.; Grassian, V.H. Titanium dioxide photocatalysis in atmospheric chemistry. *Chem. Rev.* **2012**, *112*, 5919–5948. [[CrossRef](#)] [[PubMed](#)]
34. Laufs, S.; Burgeth, G.; Duttlinger, W.; Kurtenbach, R.; Maban, M.; Thomas, C.; Wiesen, P.; Kleffmann, J. Conversion of nitrogen oxides on commercial photocatalytic dispersion paints. *Atmos. Environ.* **2010**, *44*, 2341–2349. [[CrossRef](#)]
35. Gómez Alvarez, E.; Sörgel, M.; Gligorovski, S.; Bassil, S.; Bartolomei, V.; Coulomb, B.; Zetzsch, C.; Wortham, H. Light-induced nitrous acid (HONO) production from NO<sub>2</sub> heterogeneous reactions on household chemicals. *Atmos. Environ.* **2014**, *95*, 391–399. [[CrossRef](#)]
36. Gandolfo, A.; Rouyer, L.; Wortham, H.; Gligorovski, S. The influence of wall temperature on NO<sub>2</sub> removal and HONO levels released by indoor photocatalytic paints. *Appl. Catal. B Environ.* **2017**, *209*, 429–436. [[CrossRef](#)]
37. Liu, J.; Li, S.; Mekić, M.; Jiang, H.; Zhou, W.; Loisel, G.; Song, W.; Wang, X.; Gligorovski, S. Photoenhanced Uptake of NO<sub>2</sub> and HONO Formation on Real Urban Grime. *Environ. Sci. Technol. Lett.* **2019**, *6*, 413–417. [[CrossRef](#)]
38. Laufs, S.; Cazaunau, M.; Stella, P.; Kurtenbach, R.; Cellier, P.; Mellouki, A.; Loubet, B.; Kleffmann, J. Diurnal fluxes of HONO above a crop rotation. *Atmos. Chem. Phys.* **2017**, *17*, 6907–6923. [[CrossRef](#)]
39. Sörgel, M.; Trebs, I.; Wu, D.; Held, A. A comparison of measured HONO uptake and release with calculated source strengths in a heterogeneous forest environment. *Atmos. Chem. Phys.* **2015**, *15*, 9237–9251. [[CrossRef](#)]
40. Li, X.; Brauers, T.; Häsel, R.; Bohn, B.; Fuchs, H.; Hofzumahaus, A.; Holland, F.; Lou, S.; Lu, K.D.; Rohrer, F.; et al. Exploring the atmospheric chemistry of nitrous acid (HONO) at a rural site in Southern China. *Atmos. Chem. Phys.* **2012**, *12*, 1497–1513. [[CrossRef](#)]
41. Arens, F.; Gutzwiller, L.; Baltensperger, U.; Gäggeler, H.W.; Ammann, M. Heterogeneous reaction of NO<sub>2</sub> on diesel soot particles. *Environ. Sci. Technol.* **2001**, *35*, 2191–2199. [[CrossRef](#)] [[PubMed](#)]

42. Han, C.; Yang, W.; Yang, H.; Xue, X. Enhanced photochemical conversion of NO<sub>2</sub> to HONO on humic acids in the presence of benzophenone. *Environ. Pollut.* **2017**, *231*, 979–986. [[CrossRef](#)]
43. Lee, J.D.; Whalley, L.K.; Heard, D.E.; Stone, D.; Dunmore, R.E.; Hamilton, J.F.; Young, D.E.; Allan, J.D.; Laufs, S.; Kleffmann, J. Central London HONO budget analysis Detailed budget analysis of HONO in central London reveals a missing daytime source Central London HONO budget analysis. *Atmos. Chem. Phys. Discuss* **2015**, *15*, 22097–22139. [[CrossRef](#)]
44. Ren, X.; Harder, H.; Martinez, M.; Leshner, R.L.; Oligier, A.; Simpas, J.B.; Brune, W.H.; Schwab, J.J.; Demerjian, K.L.; He, Y.; et al. OH and HO<sub>2</sub> chemistry in the urban atmosphere of New York City. *Atmos. Environ.* **2003**, *37*, 3639–3651. [[CrossRef](#)]
45. Liu, Z.; Wang, Y.; Costabile, F.; Amoroso, A.; Zhao, C.; Huey, L.G.; Stickel, R.; Liao, J.; Zhu, T. Evidence of aerosols as a media for rapid daytime HONO production over China. *Environ. Sci. Technol.* **2014**, *48*, 14386–14391. [[CrossRef](#)]
46. Hendrick, F.; Müller, J.-F.; Clémer, K.; Wang, P.; De Mazière, M.; Fayt, C.; Gielen, C.; Hermans, C.; Ma, J.Z.; Pinardi, G.; et al. Atmospheric Chemistry and Physics Four years of ground-based MAX-DOAS observations of HONO and NO<sub>2</sub> in the Beijing area. *Atmos. Chem. Phys.* **2014**, *14*, 765–781. [[CrossRef](#)]
47. Wang, L.; Wen, L.; Xu, C.; Chen, J.; Wang, X.; Yang, L.; Wang, W.; Yang, X.; Sui, X.; Yao, L.; et al. HONO and its potential source particulate nitrite at an urban site in North China during the cold season. *Sci. Total Environ.* **2015**, *538*, 93–101. [[CrossRef](#)] [[PubMed](#)]
48. Saylor, R.D. The Atmospheric Chemistry and Canopy Exchange Simulation System (ACCESS): Model description and application to a temperate deciduous forest canopy. *Atmos. Chem. Phys.* **2012**, *13*, 693–715. [[CrossRef](#)]
49. Li, J.G. A multiple-cell flat-level model for atmospheric tracer dispersion over complex terrain. *Boundary-Layer Meteorol.* **2003**, *107*, 289–322. [[CrossRef](#)]
50. Tapp, M.C.; White, P.W. A non-hydrostatic mesoscale model. *Q. J. R. Meteorol. Soc.* **1976**, *102*, 277–296. [[CrossRef](#)]
51. Na, K. Determination of VOC source signature of vehicle exhaust in a traffic tunnel. *J. Environ. Manag.* **2006**, *81*, 392–398. [[CrossRef](#)] [[PubMed](#)]
52. Bae, M.-S.; Lee, T. *Study on Risk Assessment of Vehicle Emission on the Road—Based on the Tunnel Study*; NIER Report; Ministry of Environment of Korea: Seoul, Korea, 2018; pp. 42–45.